American Mineralogist, Volume 111, pages 491–499, 2026

Raman spectroscopic investigation of ianthinite $[U_2^{4+}(UO_2)_4O_6(OH)_4(H_2O)_4]\cdot 5H_2O$, a rare mixed-valence uranium oxide hydrate

Tyler L. Spano[1,*], Travis A. Olds[2,†], Addison Malone[1], Brodie S. Barth[1,3,‡], Nicholas M. Kaitschuck[1,4,§], Jennifer N. Neu[1,‖], Daniel E. Felton[1,#], and Andrew Miskowiec[1,**]

[1]Nuclear Nonproliferation Division, Oak Ridge National Laboratory, Oak Ridge, Tennessee 37830, U.S.A.
[2]Carnegie Museum of Natural History, Pittsburgh, Pennsylvania 15213, U.S.A.
[3]Department of Civil and Environmental Engineering and Earth Sciences, University of Notre Dame, Notre Dame, Indiana 46556, U.S.A.
[4]Walker Department of Mechanical Engineering, University of Texas at Austin, Austin, Texas 78712, U.S.A.

Abstract

Ianthinite ($[U_2^{4+}(UO_2)_4O_6(OH)_4(H_2O)_4]\cdot 5H_2O$) is an exotic mineral that possesses U in both tetravalent and hexavalent oxidation states and is structurally related to the U_3O_8 polymorphs, which are commonly encountered technogenic materials in the nuclear fuel cycle. Despite the similarities between U_3O_8 and ianthinite, and the importance of ianthinite in U paragenesis, no Raman spectra have been reported for this mineral. To gain a more complete understanding of how structural attributes of ianthinite give rise to observable spectroscopic features and how these may relate to important materials in the nuclear fuel cycle, we provide, for the first time, Raman spectra of ianthinite. Ianthinite readily oxidizes at ambient conditions, complicating analysis of phase-pure material. Several analytical methods are employed herein to decouple the Raman features of ianthinite from its alteration product(s). First, a simple difference spectrum is presented, then results of Raman spectroscopic mapping are employed, and finally, we use a novel processing and analysis method. Each analysis method provides different insight into structural features that are unique to ianthinite, in particular, features that are attributable to U(IV) in distorted octahedral coordination in both ianthinite and U_3O_8 phases.

Keywords: Ianthinite, uranium mineralogy, Raman spectroscopy, U_3O_8

Introduction

Ianthinite ($[U_2^{4+}(UO_2)_4O_6(OH)_4(H_2O)_4]\cdot 5H_2O$) (Burns et al. 1997) is a rare mineral phase possessing U in both tetravalent and hexavalent oxidation states in an identical anion topology to technogenic U_3O_8, which appears throughout the nuclear fuel cycle (Miskowiec et al. 2019, 2020, 2022). The structural accommodation of multiple U valence states, as seen in ianthinite, is exceedingly rare, and ianthinite is the only known mineral species that contains essential U(IV) and U(VI). Of the hundreds of reported minerals that contain U as an essential structural component (Lussier et al. 2016), ianthinite, wyartite ($CaU^{5+}(UO_2)_2(CO_3)O_4(OH)\cdot 7H_2O$) (Guillemin and Protas 1959; Burns and Finch 1999; Hawthorne et al. 2006), wyartite-II (so-called dehydrated wyartite) ($CaU^{5+}(UO_2)_2(CO_3)O_4(OH)\cdot 3H_2O$), nollmotzite ($Mg[U^{5+}(UO_2)_2O_4F_3]\cdot 4H_2O$) (Plášil et al. 2018), richetite ($(Fe^{2+},Mg)_{0.5}Pb_{4.5}[U^{5+}(UO_2)_{17}O_{18}(OH)_{14}]\cdot\sim 19.5H_2O$) (Burns 1998; Plášil 2017), and the recently described shinkolobweite ($Pb_{1.333}[U^{5+}O(OH)(UO_2)_5O_{4.67}(OH)_{5.33}]\cdot 5H_2O$) (Olds et al. 2023), are currently the only minerals known to possess U in multiple valence states (Olds et al. 2023). Interestingly, all mixed-valence U minerals possess structural units associated with either the α- or β-U_3O_8 anion topology (Burns 2005), or, in the case of shinkolobweite, a modulated structure with a mixture thereof (Olds et al. 2023). The propensity of mixed-valence minerals and technogenic phases to adopt U_3O_8 anion topologies suggests that this structural unit is accommodating the differences in U coordination chemistry associated with varied oxidation states, and as such, may have significant implications for incorporating transuranic elements upon oxidation of used nuclear fuel (Miller et al. 1997).

Recent computational and experimental investigations into structural features of the U_3O_8 polymorphs, which possess mixed U(V) and U(VI) sites (~2:1), have elucidated exotic lattice dynamics and electronic and magnetic properties. Perhaps most interestingly, U_3O_8 undergoes a continuous solid-solid phase transition upon heating, ending near 300 °C, from *Amm*2 to $P\bar{6}2m$. During this transition, the number of crystallographically independent U sites is reduced from two to one. As a result, the mixed U(V) and U(VI) valence in the $P\bar{6}2m$ phase approaches a single intermediate valence (effective charge of $-16/3\ e^-$). Miskowiec et al. discussed this transition in detail, finding no evidence of superlattice ordering (time-independent U charge ordering), suggesting a time-dependent (dynamic) valence of the U sites (Miskowiec et al. 2020). Using neutron scattering, they found evidence of a quasielastic scattering term related to the lattice response to dynamic uranium valence, as well as a new magnetic ordering at low temperature, wherein

* Corresponding author E-mail: spanotl@ornl.gov Orcid https://orcid.org/0000-0001-6572-9722
† Orcid https://orcid.org/0000-0001-5333-0802
‡ Orcid https://orcid.org/0000-0002-5614-2601
§ Orcid https://orcid.org/0009-0008-6803-9506
‖ Orcid https://orcid.org/0000-0003-4392-349X
Orcid https://orcid.org/0000-0003-0508-2466
** Orcid https://orcid.org/0000-0002-0361-2614

0003-004X/26/0003–491$05.00/DOI: https://doi.org/10.2138/am-2025-9759

U_3O_8 exhibits antiferromagnetic ordering along the [0.5 1 1] lattice direction (Miskowiec et al. 2021). To this last point, the discovery of the [0.5 1 1] magnetic ordering configuration represented a deviation from past theoretical investigations (Yun et al. 2011; Wen et al. 2013; Brincat et al. 2015; Ranasinghe et al. 2020; Isbill et al. 2022). Given the commensurateness of the anion topology in ianthinite, previous studies on the electronic properties of U_3O_8 may be pertinent to our understanding of observable spectroscopic features related to structural attributes of U_3O_8 and analogous materials. Relatedly, an investigation into the structural and spectroscopic character of ianthinite may provide new insight into mixed valence U materials within the nuclear fuel cycle, such as U_3O_8.

Despite the importance of ianthinite as a natural analog to U_3O_8 anion topologies, in paragenetic sequences of U alteration, and the predisposition of this phase to form during alteration of used nuclear fuel (Taylor et al. 1991), no optical vibrational spectroscopic data have been reported for ianthinite. For the first time, we provide Raman spectra for ianthinite, describe the structural origins of spectroscopic features, and assess spectroscopic features that are common between ianthinite and the topologically identical technogenic phase β-U_3O_8 and the structurally similar α-U_3O_8. One challenge associated with the analysis of ianthinite is the tendency for oxidation and alteration of this phase. At ambient conditions, ianthinite readily transforms to schoepite and/ or metaschoepite, complicating detailed spectroscopic characterization of this phase (Finch and Murakami 1999). To overcome this challenge, we employ spatially resolved optical vibrational spectroscopic techniques to detail the unique features of the Raman spectra of ianthinite relative to its alteration phase(s). Using a novel analysis method, we also describe potential crystal chemical origins of spectroscopic differences and find that the most likely source of spectroscopic variability is related to differences in connectivity between the bonding behavior of axial U-O_{yl} O atoms between the structural unit of ianthinite, and charge-balancing interstitial complexes.

Materials and Methods

Ianthinite Samples and Geologic Setting

The structure of ianthinite was determined by Burns et al. (1997) from a crystal extracted from the Shinkolobwe (Kasolo) mine in Shaba, Democratic Republic of the Congo. In that work, Burns et al. (1997) provide a detailed summary of previous work on this mineral species. Briefly, ianthinite always occurs in close proximity to primary uraninite and is often associated with uranyl oxyhydroxide-hydrate minerals such as schoepite and becquerelite. At ambient conditions, ianthinite oxidizes to schoepite or metaschoepite, with the alteration products often referred to by their pseudonym, "epi-ianthinite." Although some recent studies have been done on the formation mechanisms of ianthinite in an Indian locality in Andhra Pradesh (Singh et al. 2014), the overall mode of occurrence remains understudied given the importance of ianthinite in paragenetic sequences of U alteration, and the similarities between this mineral and technogenic phases encountered in the nuclear fuel cycle.

A sample of ianthinite from the Shinkolobwe mine, Democratic Republic of the Congo, provided by the Carnegie Museum of Natural History, was examined in this work.

Powder X-ray Diffraction

X-ray diffraction (XRD) data for powdered ianthinite and oxidized ianthinite (metaschoepite) from the Shinkolobwe mine were obtained using a Bruker Apex II equipped with Photon III CPAD detector and IμS2.0 microfocus source with monochromatized Mo$K\alpha$ radiation (0.71069 Å). A pseudo-Gandolfi motion on the ϕ and ω axes was used to randomize diffraction from the samples. Unit-cell parameters refined from the powder XRD data (Online Materials[1] Fig. S1) using JADE Pro (Materials Data, Inc.) with whole pattern fitting based on known structures confirmed the identities of the minerals studied. For ianthinite (Burns et al. 1997), they are: space group $P2_1cn$, $a = 7.20(1)$ Å, $b = 11.05(1)$ Å, $c = 29.65(6)$ Å, $V = 2359$ Å^3. For oxidized ianthinite [metaschoepite; (Klingensmith et al. 2007)] space group *Pbcn:* $a = 15.08(2)$ Å, $b = 14.56(2)$ Å, $c = 16.53(2)$ Å, $V = 3628$ Å^3.

Raman Spectroscopy

A Renishaw inVia micro-Raman spectrometer was used to collect data for samples of ianthinite, which were adhered to carbon tabs. An excitation wavelength of 785 nm was used to collect spectra in the range of 35–1200 cm^{-1} in combination with a 1200 L/mm holographic notch diffraction grating and resulting spectral resolution of ~2.5–3.1 cm^{-1}. Corresponding power densities of Raman measurements were ~100 W/cm^2 based upon laser power (10 mW) and spot size (~1 μm). Reported spectra are the sum of 20 accumulations, each with a 10 s exposure time.

To examine potential spectroscopic variability associated with the oxidation of ianthinite to schoepite/metaschoepite, we collected a Raman spectroscopic map on an area of the ianthinite sample that was visually identified as a transition zone between the mixed-valence phase and the U(VI) alteration product based on the presence of dark and light crystalline aggregates. To do this, we collected spectra every 3 μm in an 18 × 14 grid (252 total points). Each point was measured using 10 accumulations with a 10 s exposure time at 100 W/cm^2. Average photon counts were ~2000 counts/cm^{-1}, such that random noise levels were negligible. To analyze the data, we examined intensity ratios between three observed peaks in the range of 800–900 cm^{-1} to explore differences in uranyl mode contributions. We also calculated the mean Raman spectra across all data sets; then, calculated the standard deviation of the spectral intensity at each Raman shift bin as extracted from a normal distribution fit of the intensity histogram. We expect that if there are significant chemical differences within the map that specific regions of the spectra will show substantially higher standard deviation from the mean.

Non-negative least squares regression analysis, done in the WiRE software package, was also employed to elucidate Raman spectroscopic features of ianthinite from its oxidation products. We used point spectra collected on areas of the sample that appeared visually altered, as indicated by a bright yellow color, in addition to point spectra on the dark-violet regions of the sample that are consistent with the reported appearance of ianthinite as spectroscopic end-members. We note that there was no apparent change in crystallinity or crystallographic orientation between altered and unaltered regions of the sample (e.g., Fig. 1). Using the Raman spectroscopic map data collected for the transition region described above, we calculated contributions to each spectral data set from the altered and unaltered end-members.

Scanning Electron Microscopy with Energy-Dispersive X-ray Spectroscopy and X-ray Fluorescence Spectroscopy

Scanning electron microscopic (SEM) images were collected using a Zeiss Gemini 460 field emission SEM to explore crystal morphology of ianthinite samples adhered to carbon tabs (Online Materials[1] Fig. S2). Backscatter electron images were collected using an accelerating voltage of 20 kV and currents of 94–200 pA. Micro-X-ray fluorescence spectroscopy was employed to image the spatial distribution of elemental contributions on the specimens of ianthinite (Online Materials[1] Fig. S3). This measurement was done using an IXRF Atlas instrument, equipped with a motorized stage, 50 kV/50W/ 1 mA Rh X-ray tube with a 5 μm spot size, polycapillary focusing optic, and four silicon drift detectors. Samples were analyzed in a light-tight chamber under vacuum for element detection to Ca.

Results and Discussion

Spectroscopic Features and Their Structural Origins

We began our investigation of ianthinite by collecting Raman spectra for numerous individual crystals, with representative spectra shown in Figure 1. For Raman measurements, we examined crystals that appeared dark violet-brown, as this is consistent with the reported appearance of ianthinite, although significant alteration is indicated in our sample by the presence of bright yellow

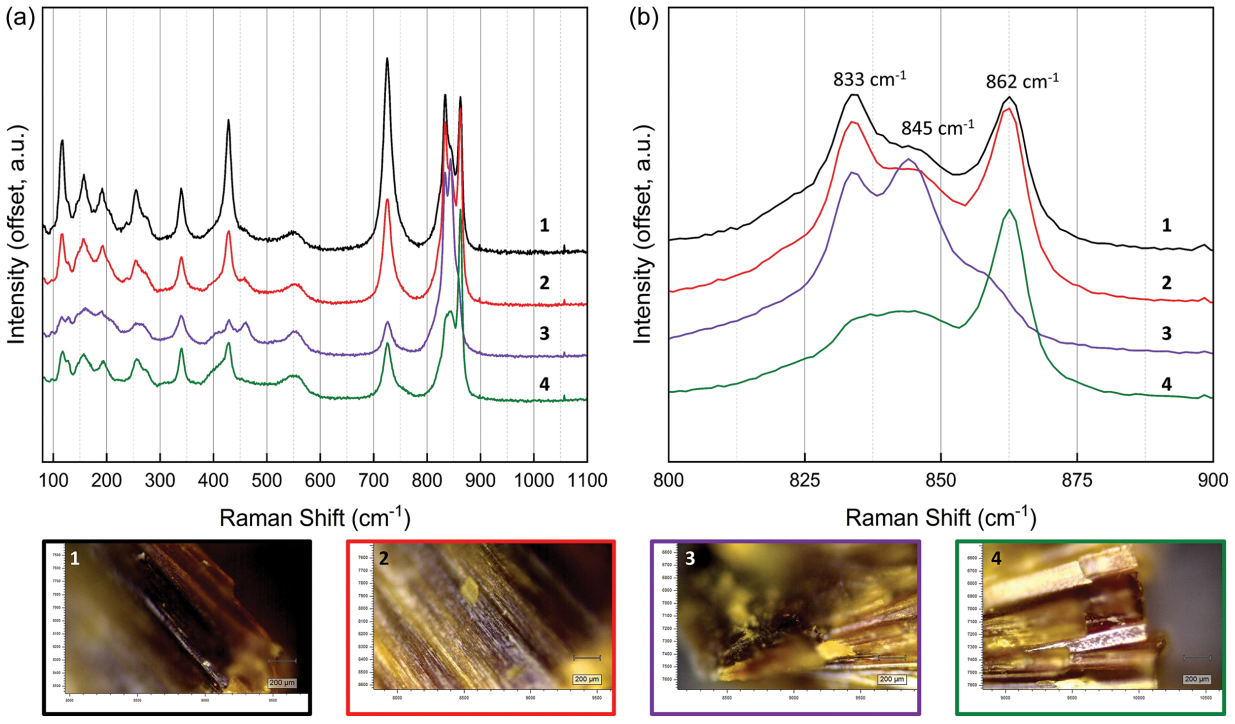

Figure 1. (**a**) Example Raman spectra collected for several crystals of ianthinite on a specimen from Shinkolobwe. (**b**) Significant differences in relative spectroscopic intensity are observed in the range of 800–900 cm^{-1}, the region associated with symmetric stretching vibrations of axial uranyl O. Numbered images below the spectra correspond to data shown in (**a**) and (**b**) and have corresponding colored borders. Spectra are offset for clarity. (Color online.)

areas of material. We also collected spectra for areas of the sample that appeared significantly altered and will discuss later how we used these data to elucidate spectral contributions from ianthinite and its alteration phases. In addition to the example data sets shown in Figure 1, numerous other data sets for visibly unaltered ianthinite were collected (see Online Materials[1]), and we calculated an average spectrum (n = 15) from these data sets following a 0,1 normalization of data to account for intensity differences and provide an average Raman spectrum for ianthinite (Fig. 2). This average spectrum was then fit to Voigt peaks using a Levenberg-Marquardt nonlinear least squares method in the Fityk software package (Wojdyr 2010) to further analyze spectroscopic features. Proposed band assignments for the Raman spectra of ianthinite are found in Table 1.

In the Raman spectra of ianthinite, between 800 and 900 cm^{-1}, numerous apparent vibrational modes are observed (Figs. 1b and 2). All spectra appear to show a peak centered at 845 cm^{-1}, with both, or either, high and low energy shoulders centered at 862 and 833 cm^{-1}, respectively (Fig. 1b). Vibrational modes in this region are attributable to the ν_1 symmetric stretching vibration associated with the axial U-O (uranyl, U-O_{yl}) bonds which are abundant in U(VI) phases (Bartlett and Cooney 1989; Lu et al. 2018; Spano et al. 2023). The multiple peaks in our spectra are attributable to multiple crystallographically distinct uranyl units within the structure of ianthinite, and perhaps, varying degrees of alteration from ianthinite to its oxidation products. Although ianthinite possesses the β-U_3O_8 anion topology, the namesake of which possesses three unique U sites, ianthinite has six independent U sites in its asymmetric unit and displays alternating basal layers of U-O sheets (Fig. 3), making it structurally distinct from the technogenic U oxide. Two symmetrically independent

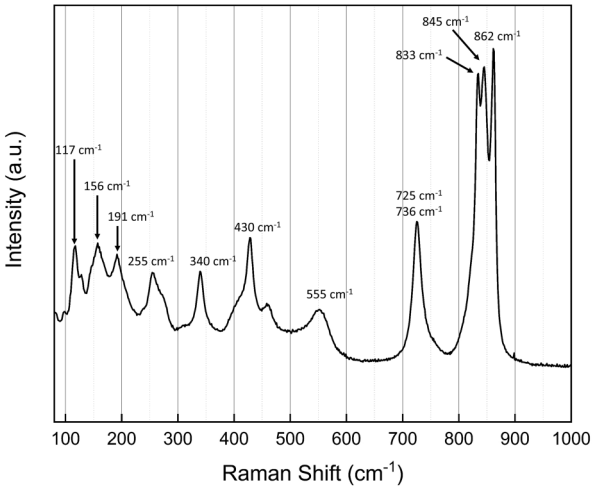

Figure 2. The average Raman spectrum of ianthinite from Shinkolobwe in the range of 80–1000 cm^{-1}. The average spectrum was calculated from 15 individual data sets collected for Shinkolobwe ianthinite. The most notable features are a complex multiplet of modes in the uranyl symmetric stretching region (~800–900 cm^{-1}) and an asymmetric band centered at 725 cm^{-1}, which originates from symmetric stretching of distorted octahedral coordination units of U(IV).

Table 1. Proposed spectroscopic assignments for ianthinite

Feature (cm^{-1})	Assignment	Notes	Reference
862	ν_1U(VI)-O stretching	Primarily associated with altered ianthinite	This work
845	ν_1U(VI)-O stretching	Primarily associated with altered ianthinite	This work
833	ν_1U(IV, VI)-O stretching	Associated with altered and unaltered ianthinite	This work
725	ν_1U(VI)-O stretching	Primarily associated with unaltered ianthinite	This work
736	ν_1U(VI)-O stretching	Primarily associated with unaltered ianthinite	This work
555	O-H bending	Associated with altered ianthinite	Colmenero et al. (2019); Kirkegaard et al. (2019a)
430	O-H stretching	Associated with unaltered ianthinite	This work; Kirkegaard et al. (2019a)
370	O-H stretching	Associated with unaltered ianthinite	This work; Kirkegaard et al. (2019a)
340	ν_1U(IV)-OH stretching	Associated with unaltered ianthinite	This work; Kirkegaard et al. (2019a)
310		Associated with altered ianthinite	This work
255	U-O/U-OH bending	Primarily associated with altered ianthinite	Kirkegaard et al. (2019a)
191	U(IV)-O bending	Associated with altered ianthinite	Kirkegaard et al. (2019a)
156	U(IV, VI)-O bending	Associated with altered and unaltered ianthinite	Kirkegaard et al. (2019a)
117		Associated with unaltered ianthinite	This work

U-O/OH sheets form the structural unit in ianthinite. Both sheets adopt the β-U_3O_8 anion topology, where edge-sharing chains of pentagonal bipyramidal U units interlink through edge sharing of distorted U-centered octahedra (U2 and U4) and vertex sharing between pentagonal bipyramids of next-neighbor chains, forming "bow-tie" voids. In the first sheet, shown in Figure 3a, edge-sharing chains of pentagonal bipyramids (U1) link through vertex sharing to neighboring U3 chains. Conversely, the second sheet (Fig. 3b) contains edge-sharing chains of alternating pentagonal bipyramids formed from the U5 and U6 sites. These two U oxide sheets are connected via hydrogen bonding from interstitial water (Fig. 3c). Sheets are stacked in an offset fashion (Fig. 3d), in which pentagonal bipyramidal chains stack above rows of distorted octahedra.

According to bond-valence analysis by Burns et al. (1997), U sites in pentagonal bipyramidal coordination are U(VI), and, as a result, contribute to the complexity of features observed in the uranyl region, between 800 and 850 cm^{-1}. Using the correlation between U-O_{yl} bond length and position of the ν_1 symmetric stretching vibrational mode in Raman spectra described by Bartlett and Cooney (1989), we indeed see excellent agreement between bond length and position of this mode. The three peaks seen at 862, 845, and 833 cm^{-1} should correspond to uranyl bond lengths of 1.75, 1.76, and 1.77 Å, respectively. This is consistent with the ianthinite structure provided by Burns et al. (1997), where U-O_{yl} bonds range from 1.76–1.80 Å.

Based on bond-valence analysis from the structure description provided by Burns et al., the octahedrally coordinated U are

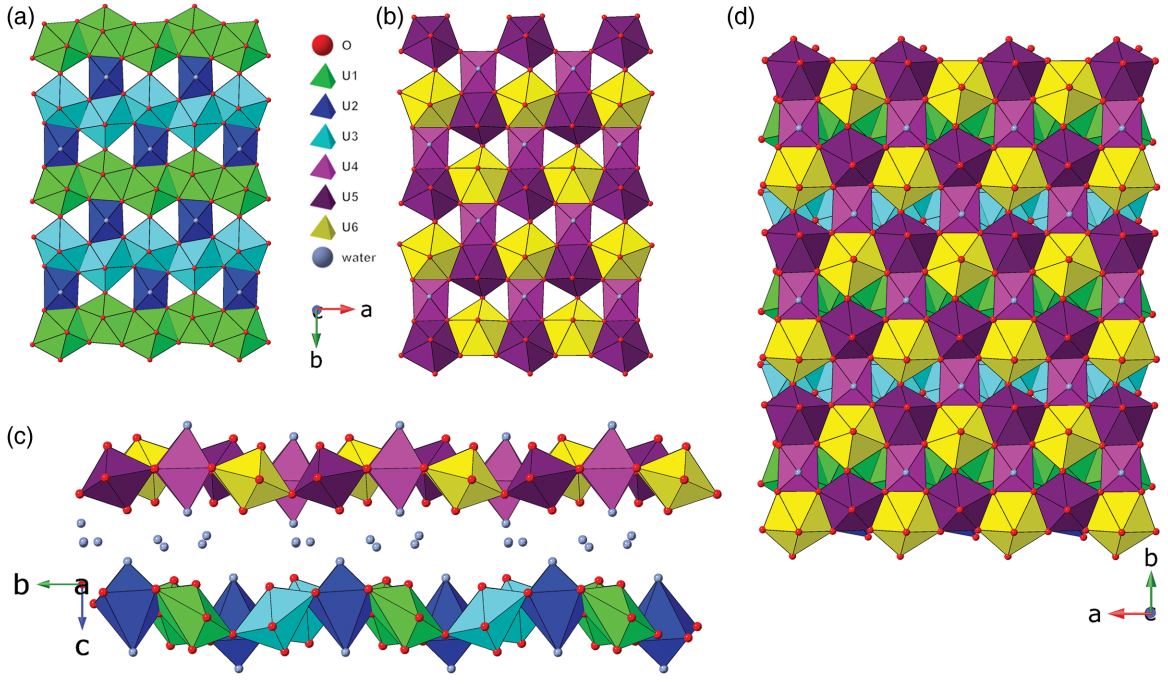

Figure 3. The crystal structure of ianthinite. (**a**) The first of two structural unit sheets that shows two chains (cyan and green) of crystallographically independent uranyl pentagonal bipyramids linked through distorted U(IV) octahedra (blue). (**b**) The second structural unit sheet in ianthinite, where alternating U sites (yellow, purple) make up chains of pentagonal bipyramids linked through distorted U(IV) octahedra (fuchsia). (**c**) Stacking of U-O sheets viewed down a. Interstitial water atoms are shown as gray spheres. (**d**) Stacking of sheets viewed down c. (Color online.)

likely U(IV), and do not contain U-O_{yl} bonds, instead forming long (~2.4 Å) axial bonds to H_2O groups. However, symmetric stretching of slightly shorter equatorial U-O/OH bonds (~2.0–2.2 Å) may exhibit "uranyl-like" behavior and be the origin of the intense vibrational mode observed at 725 cm^{-1}. Notably, the distorted octahedral sites in ianthinite possess slight differences in U-O bond lengths. Two short (relative to the remaining 4 U-O bond distances) bonds are found in each distorted octahedral site, with U-O lengths of 1.96 and 2.00 Å in U2, and 2.05 and 2.18 Å in U4. If the intense mode at 725 cm^{-1} originates from U-O symmetric stretching of the distorted octahedral U, we would expect to see more than a singular mode here, given the presence of two U sites with this distorted octahedral coordination environment, and/or the inequivalent short U-O bond lengths about each site. Thinking of U-O bonds as harmonic oscillators, the Raman signal associated with vibrations of longer bonds appears at lower energy than that of shorter, stronger bonds. Following peak fitting of the average spectrum of ianthinite shown in Figure 2, we observe that two peaks contribute to the observed intensity at 725 cm^{-1}, with a second, low-intensity peak at 736 cm^{-1}. The presence of this second feature may arise from either the second crystallographically distinct distorted octahedron (e.g., one mode originates from U2, the other from U4, Fig. 3), or from variability in the bond length of U-O (e.g., U2 and U4 each have two distinct "short" U-O bonds). Nevertheless, the presence of two peaks strongly indicates that the vibrational modes between 725 and 750 cm^{-1} are a unique signature of U(IV) in octahedral coordination.

Upon comparison of the spectrum of ianthinite to α- and β-U_3O_8 (Fig. 4), we see a similar feature in the technogenic U oxide phases. In both α- and β-U_3O_8, this feature is centered at 750 cm^{-1} (Miskowiec et al. 2019, 2022). However, in α-U_3O_8, the 750 cm^{-1} peak is quite diffuse, and is almost entirely Gaussian in character (Miskowiec et al. 2019). β-U_3O_8, conversely, has a sharper 750 cm^{-1} peak, which is entirely Lorentzian (Miskowiec et al. 2022). Given the topological isomorphism between ianthinite and β-U_3O_8, one may expect to see similar behavior of bands in the region of 725–750 cm^{-1}, and to this end we analyzed the two vibrational modes that contribute to the apparent feature at ~725 cm^{-1} in the average Raman spectrum of ianthinite (Fig. 2) using the same method as Miskowiec et al. (2019). From our fitting results (Online Materials[1] Table S1) the more intense peak (725 cm^{-1}) in the Raman spectrum of ianthinite (Fig. 2) is ~50% Gaussian and 50% Lorentzian in character. Conversely, the higher energy, lower intensity feature, centered at 730 cm^{-1}, is purely Lorentzian. The purely Lorentzian peak at 730 cm^{-1} in the Raman spectrum of ianthinite indicates that dynamic phonon relaxation mechanisms may be operative for this band, rather than a convolution of dynamic (Lorentzian) and structural (Gaussian) effects as observed for the more intense vibrational mode in this region at 725 cm^{-1}. Time-dependent phonon relaxation, indicated by Lorentzian bands or components in the Raman, may be attributable to defect or grain-boundary scattering, or phonon-phonon/electron-phonon interactions. Although we cannot definitively ascribe a specific relaxation process to the Lorentzian bands, we do note the similar character between peaks in both β-U_3O_8 and ianthinite, which we attribute to vibrational modes associated with lower valence U in distorted octahedral coordination.

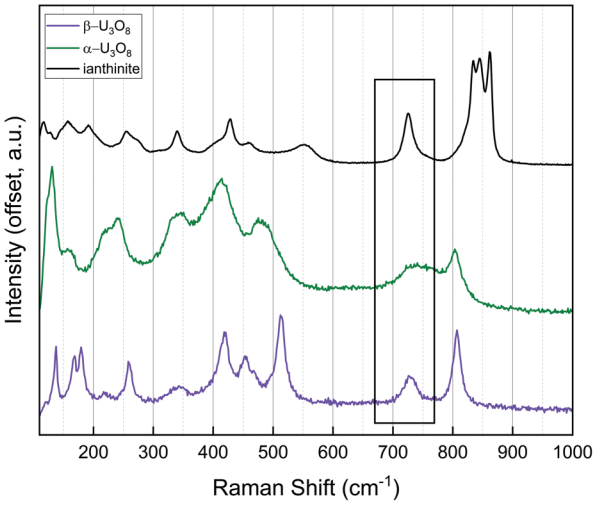

FIGURE 4. The average Raman spectrum of ianthinite compared with structurally similar technogenic U phases, α- and β-U_3O_8 in the green and purple traces, respectively. The box overlaid on the spectra shows specific features that may be indicative of U(IV) in octahedral coordination. Of note, the highlighted band, centered at 725 cm^{-1} is more diffuse in α-U_3O_8 relative to its appearance in β-U_3O_8 and ianthinite the latter of which adopts the β-U_3O_8 anion topology. (Color online.)

At lower energy, consistent spectral features are seen for most data sets, with well-resolved peaks observed at 117, 156, 191, 255, 340, and 430 cm^{-1} in all spectra (Fig. 1). Most peaks in this region are associated with U-O equatorial stretching and bending motions based on assignments for shinkolobweite provided by Olds et al. (2023). The additional complexity here, as was observed in the uranyl region, results from the numerous equatorial coordination modalities that arise from the multiple distinct U environments in ianthinite. In addition to the well-resolved equatorial modes, several diffuse spectral features are observed. We see a broad band with lower intensity relative to other spectroscopic features centered at 555 cm^{-1}, and shoulder modes at ~310 and 370 cm^{-1} are present in some spectra. The peak at 555 cm^{-1} may be attributable to O-H bending of water molecules that decorate U-O structural units based on assignments for similar species from the literature (Colmenero et al. 2019; Kirkegaard et al. 2019a), and we would expect to see variability in the intensity and position of this band when comparing Raman spectra of ianthinite with its alteration products.

Decoupling the Raman Spectrum of Ianthinite from Alteration Species

Given ianthinite's propensity to degrade to schoepite and/ or metaschoepite under ambient conditions, we explored several methods to isolate the Raman spectrum of the mixed valence phase from its alteration species. Although separating the spectroscopic features of ianthinite from its alteration products may not be strictly necessary from a mineralogical perspective (e.g., for identification of this mineral via Raman, most natural samples are likely altered, as our material is), we examined features of ianthinite through the lens of U_3O_8 phases and identified commonalities

therebetween. To facilitate comparison of ianthinite and U_3O_8, we first tried a simple "background" subtraction on normalized data. Second, we used spectroscopic mapping to determine the spatial distribution of spectroscopic features. Finally, we took a mathematical approach to analyze hundreds of data sets collected during spectroscopic mapping. Some of these techniques were more successful than others in elucidating the spectrum of unaltered ianthinite, but each provided unique insight into structure-property relationships and is described below.

To remove potential spectroscopic features of alteration phases from the Raman spectrum of ianthinite, a "background" subtraction was attempted. This subtraction was done by taking a spectrum (Fig. 5a) collected on a visibly altered bright yellow area of our specimen (Fig. 5b), performing a 0,1 normalization, and subtracting this unaltered spectrum from the average ianthinite spectrum that was normalized in the same way. Of note, the average spectrum of the alteration phase shown in Figure 5a is in excellent agreement with features associated with synthetic metaschoepite, albeit with slight shifts in position of one symmetric stretching vibrational mode, but does not correlate with those of schoepite (Online Materials[1] Fig. S4). The resulting difference spectrum shown in Figure 5a shows significant negative spectral contributions at ~858 cm^{-1}, indicating that spectroscopic intensity is shared between alteration phases and ianthinite here. Notably, this background subtraction method highlights that the peak located at 725 cm^{-1} is indeed related to unaltered ianthinite and furthers our supposition that this peak originates from symmetric stretching of O of distorted U octahedra because similar spectroscopic features are observed in U_3O_8 (Fig. 4). Our assignment in the previous section, in which the peak at ~555 cm^{-1} was assigned to O-H bending modes is also indicated by the results shown in Figure 7, although we see from the difference spectrum that this diffuse band is more closely associated with alteration phases, rather than ianthinite itself. Figure 5 also shows that many of the peaks in the range of 175–300 cm^{-1} likely result largely, but not entirely, from alteration phase contributions. Despite providing some clarity regarding the Raman spectrum of unaltered ianthinite, the difference spectrum shown in Figure 5b is not sufficient to completely differentiate between alteration vs. pristine ianthinite mineral phases.

A second method involving Raman spectroscopic mapping, described in the Materials and Methods section, was attempted to help clarify spectroscopic contributions unique to ianthinite. Raman peaks in the uranyl region (~800–900 cm^{-1}) were fit with three pseudo-Voigt peaks using the WiRE software package, and peak intensities of the three constituents were mapped for a data set collected in a region of the sample that appears to show the transition between ianthinite and its alteration products (Fig. 6a). The peaks in the uranyl region determined from this method are centered at 862, 844, and 833 cm^{-1}. Unsurprisingly, given the paragenetic relationship between ianthinite, schoepite, and metaschoepite, as well as our results that illustrate the coincidence of peaks in both ianthinite and its alteration phases (Fig. 5), the positions of these peaks are similar to those reported for uranyl modes associated with schoepite and metaschoepite (Colmenero et al. 2019; Kirkegaard et al. 2019b). Following peak fitting, intensity ratios were generated for each combination of peaks at 862, 844, and 833 cm^{-1}, with resulting spectroscopic ratio maps shown in Figures 6b–6d. In Figure 6b, significant intensity contributions from the vibrational mode at 833 cm^{-1} relative to the mode at 844 cm^{-1} are visible for

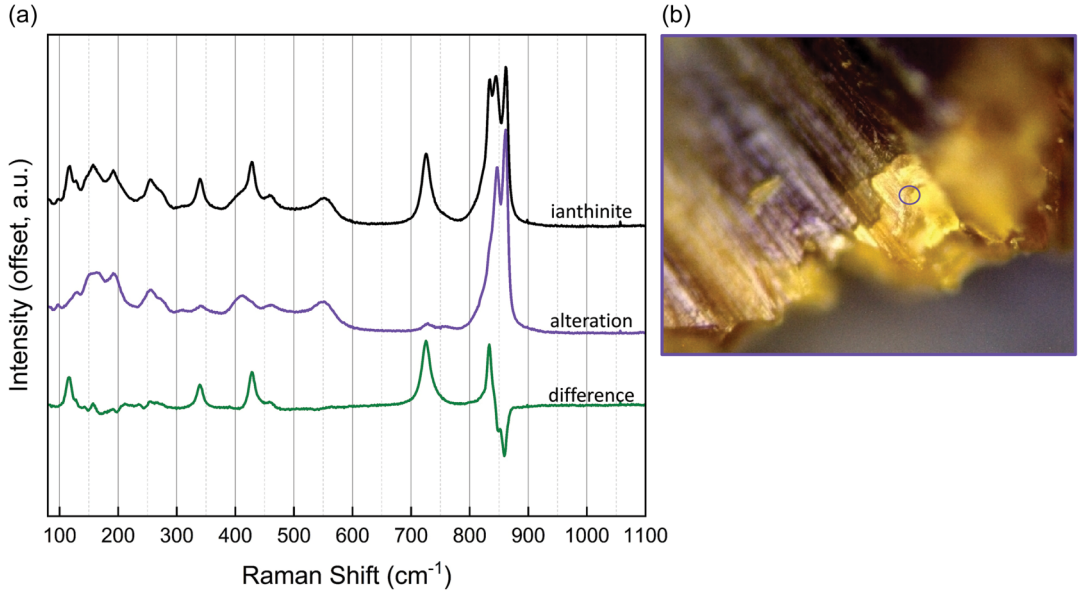

Figure 5. (**a**) Raman spectra collected for ianthinite (black trace) and a visibly altered region on the same specimen of ianthinite from Shinkolobwe (purple trace). The difference spectrum (green trace) was calculated by subtracting the spectrum collected for the visibly altered region from the average Raman spectrum of ianthinte from Shinkolobwe. Significant negative intensity is observed in the uranyl region ~860 cm^{-1}, suggesting that spectroscopic features in this region are shared between ianthinite and its alteration species. (**b**) Optical image of the visibly altered area sampled, horizontal FOV is ~300 μm. (Color online.)

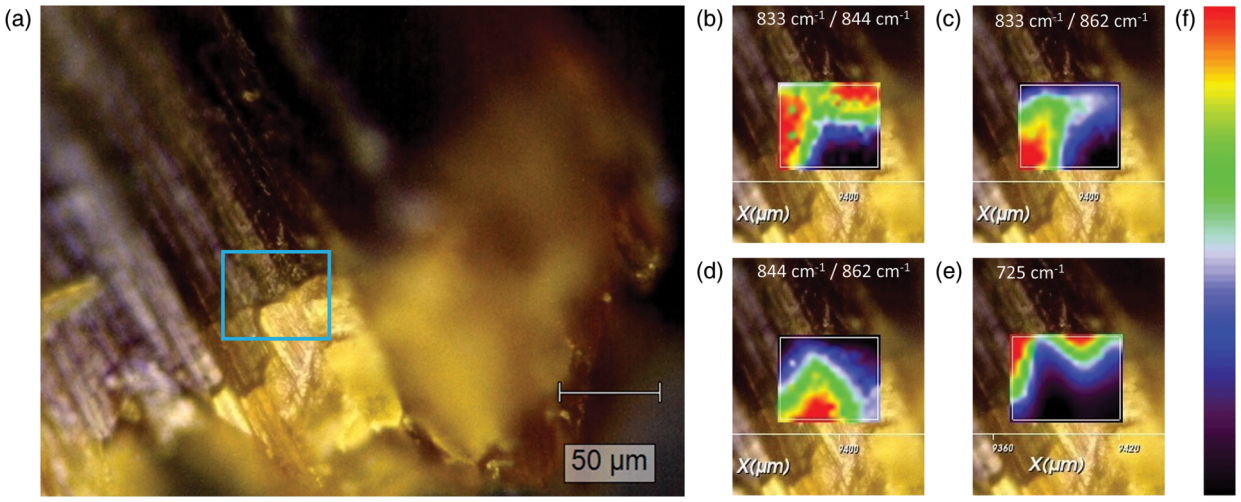

Figure 6. (a) Optical image showing the transition region of an aggregate of crystals from the ianthinite specimen, progressing from dark violet (less altered) to golden-yellow (more altered). (**b**) Intensity ratio map comparing spectroscopic features at 833 and 844 cm^{-1}. This map indicates that the feature at 833 cm^{-1} is more prominent in unaltered ianthinite. (**c**) Intensity ratio map comparing features at 833 and 862 cm^{-1}. The 833 cm^{-1} feature remains prominent, further indicating that this feature originates from unaltered ianthinite. (**d**) Intensity ratio map comparing features at 844 and 862 cm^{-1}, showing that features in this region are more closely associated with alteration phases of ianthinite. (**e**) Intensity map of a peak centered at 725 cm^{-1}, with higher intensity associated with unaltered ianthinite. (Color online.)

the portion of the sample that appears optically to be less altered. This observation is again consistent with our findings from examining the difference spectrum shown in Figure 5, in which areas of spectroscopic intensity remain at the lowest energy portion of the uranyl region of the difference spectrum upon subtraction of spectroscopic features that are more likely associated with the alteration phase. Similarly, Figure 6c indicates that the vibrational mode at 833 cm^{-1} remains prevalent when compared with the peak at 862 cm^{-1} and suggests that the 833 cm^{-1} mode is closely associated with unaltered ianthinite. When comparing the 844 cm^{-1} peak intensity to that of the 862 cm^{-1} peak, significantly higher ratios are shown for the visibly altered region of ianthinite (Fig. 6d), indicating that one or both of these peaks are attributable to altered portions of the specimen. This observation of higher energy contributions from more altered species is also in agreement with results in the difference spectrum shown in Figure 5a. To examine whether our hypothesis that the peak at ~725 cm^{-1} belongs to unaltered ianthinite is correct, we also created an intensity map of this peak (Fig. 6e). We indeed observe that spectroscopic intensity at 725 cm^{-1} is strongly correlated with visibly unaltered regions of our specimen. Although a useful tool for visualizing the spatial distribution of spectroscopic contributions and confirming that the peak at 725 cm^{-1} is a feature of unaltered ianthinite, we still find it difficult to definitively assign spectroscopic features in the uranyl region to ianthinite vs. its alteration products from this mapping experiment, thus necessitating additional analyses.

To further explore variability that may exist in the sample of ianthinite, Raman spectroscopic map data were analyzed using a novel processing method described in the Materials and Methods section that allows examination of overall intensity variability in regions of the spectra across all data sets included in spectroscopic maps described previously. In Figure 7, normalized intensity and associated variability are shown for the entire spectral range. Unsurprisingly, significant intensity differences are visible in peaks within the uranyl region (~800–900 cm^{-1}) of the spectra, indicating that inconsistencies in U-O_{yl} bond length (and bond strength) are present within the examined sample. Variability in this region is expected; as ianthinite undergoes alteration to schoepite, and/or its dehydrated counterpart metaschoepite (or a mixture thereof), significant differences in connectivity between anionic sheets of U-O polyhedra, which are linked to interstitial species via bonding between O_{yl} atoms and OH and/or H_2O within the interlayer, would lead to variance in U-O_{yl} bond strengths, bond lengths, and resultingly, in the position of the symmetric stretching vibrational modes associated with uranyl centers. Figure 7 also shows marked variability in spectroscopic peaks in the range of 150–200 cm^{-1}. From assignments of metaschoepite in the literature (Kirkegaard et al. 2019a), Table 1, vibrational modes in this region are attributable to bending modes of the uranyl ion, which may also be susceptible to slight changes resulting from differences in interlayer connectivity and, as a result, bond strength and length. Another notable observation from this analysis is that the intensity of the peak(s) located at ~725 cm^{-1} (Figs. 1, 2, 4, and 5) that we posit originates from symmetric stretching vibrations of shorter U-O bonds about distorted U(IV) octahedra (Fig. 3) is extremely variable across the map area (the same area shown in Figs. 6b–6d), as would be expected in an area of the specimen where spectroscopic contributions from ianthinite are decreasing and those from (meta)schoepite are increasing. As was hypothesized earlier in this section, variability is also visible in the intensity of the peak at ~555 cm^{-1}, indicating that differences in O-H bending of water molecules that decorate U-O structural units lead to differences in the Raman spectra of ianthinite and its alteration phases. More broadly, the results shown in Figure 7 strongly suggest that the Raman spectra of ianthinite and its alteration species exist in a continuum, where gradual phase transitions between mineral

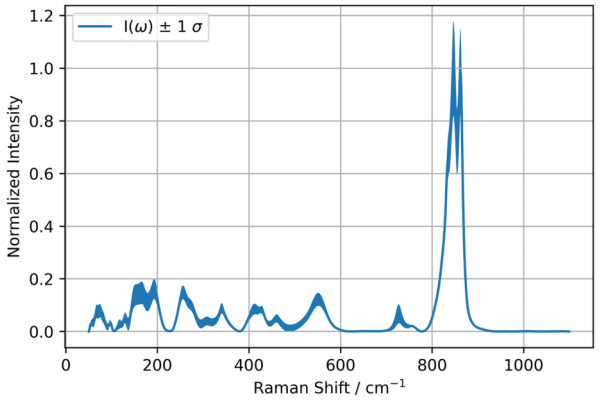

Figure 7. Average Raman spectra with intensity variations depicted as a channel plot. At each Raman shift, the mean Raman intensity is calculated, as well as the standard deviation for all intensity values at that point. The standard deviation is plotted as a positive and negative channel extent extending from the mean value. This analysis highlights regions of larger intrasample variation in the spectra, such as the region between 150 and 200 cm^{-1}. Furthermore, the Raman spectra with their intrasample variation provide a more complete picture of the overall variability of this material. (Color online.)

species result in subtle but detectable variability in the Raman spectra thereof.

Concluding Remarks

This article examines ianthinite from Shinkolobwe. For the first time, we report Raman spectra for this exotic mineral phase and describe features that are indicative of U(IV) in distorted octahedral coordination. Several methods are presented for decoupling the Raman spectrum of ianthinite from associated alteration phases. First, a difference spectrum calculated by subtracting an intensity-normalized alteration-phase spectrum from that of pristine material is presented, and from this data, we begin to see evidence of spectroscopic features of U(IV) coordination polyhedra. This difference spectrum also indicated that bands in the Raman spectrum of ianthinite are shared with those in the spectrum of alteration phases thereof. Additionally, we used Raman mapping to clarify the spatial distribution of various spectroscopic features, and further show that Raman peaks around ~725 cm^{-1} are attributable to the pristine material. Finally, we present a novel analysis method that further indicates that the spectra of ianthinite and its alteration products should be thought of as a continuum, with many shared features. Most importantly, we ascertain that similarities indeed exist between ianthinite and the structurally related technogenic U phases, α- and β-U_3O_8.

Implications

Understanding the crystal-chemical origins of spectroscopic features is a unique challenge encountered as Raman spectroscopy emerges as a state-of-practice technique for forensic analysis of nuclear materials (Schwantes et al. 2022a, 2022b). In particular, small particles, non-ideal samples that have undergone environmental degradation, and mixed-phase materials are often encountered in the field of nuclear forensics (Lin et al. 2013, 2014; Said et al. 2021). The work presented here describes multi-method techniques for determining spectroscopic features of one part of a phase mixture. Specifically, we examined ianthinite, which is a rare mixed-valence U mineral, and the only U mineral reported to contain essential U(IV) and U(VI). In addition to elucidating the structural origins of spectroscopic features of ianthinite, we present new insight into indicators of mixed valence U phases in Raman spectra through comparison with structurally related fuel cycle materials α- and β-U_3O_8, the latter of which possesses an identical anion topology to ianthinite. In addition to providing the first Raman spectra for ianthinite, comparing the Raman spectra of ianthinite to related alteration phases provides new insight into the ways in which the underlying crystal structure of a material translates into observable spectroscopic features.

Acknowledgments and Funding

This manuscript was significantly improved by helpful discussions with Avery Wood and Jordan Roach and the comments of two anonymous reviewers. This work was funded by the U.S. Department of Energy, National Nuclear Security Administration, Office of Defense Nuclear Nonproliferation R&D.

This manuscript has been authored by UT-Battelle, LLC, under contract DE-AC05-00OR22725 with the U.S. Department of Energy (DOE). The U.S. government retains, and the publisher, by accepting the article for publication, acknowledges that the U.S. government retains a nonexclusive, paid-up, irrevocable, worldwide license to publish or reproduce the published form of this manuscript, or allow others to do so, for U.S. government purposes. DOE will provide public access to these results of federally sponsored research in accordance with the DOE Public Access Plan (http://energy.gov/downloads/doe-public-access-plan).

References Cited

Bartlett, J.R. and Cooney, R.P. (1989) On the determination of uranium-oxygen bond lengths in dioxouranium (VI) compounds by Raman spectroscopy. Journal of Molecular Structure, 193, 295–300, https://doi.org/10.1016/0022-2860(89)80140-1.

Brincat, N.A., Parker, S.C., Molinari, M., Allen, G.C., and Storr, M.T. (2015) Density functional theory investigation of the layered uranium oxides U_3O_8 and U_2O_5. Dalton Transactions: An International Journal of Inorganic Chemistry, 44, 2613–2622, https://doi.org/10.1039/C4DT02493A.

Burns, P.C. (1998) The structure of richetite, a rare lead uranyl oxide hydrate. Canadian Mineralogist, 36, 187–199.

——— (2005) U^{6+} minerals and inorganic compounds: Insights into an expanded structural hierarchy of crystal structures. Canadian Mineralogist, 43, 1839–1894, https://doi.org/10.2113/gscanmin.43.6.1839.

Burns, P.C. and Finch, R.J. (1999) Wyartite: Crystallographic evidence for the first pentavalent-uranium mineral. American Mineralogist, 84, 1456–1460, https://doi.org/10.2138/am-1999-0926.

Burns, P.C., Finch, R.J., Hawthorne, F.C., Miller, M.L., and Ewing, R.C. (1997) The crystal structure of ianthinite, $[U_2^{4+}(UO_2)_4O_6(OH)_4(H_2O)_4](H_2O)_5$: A possible phase for Pu4+ incorporation during the oxidation of spent nuclear fuel. Journal of Nuclear Materials, 249, 199–206, https://doi.org/10.1016/S0022-3115(97)00212-2.

Colmenero, F., Fernández, A.M., Cobos, J., and Timón, V. (2019) Periodic DFT study of the thermodynamic properties and stability of schoepite and metaschoepite mineral phases. ACS Earth & Space Chemistry, 3, 17–28, https://doi.org/10.1021/acsearthspacechem.8b00109.

Finch, R. and Murakami, T. (1999) Systematics and paragenesis of uranium minerals. Reviews in Mineralogy and Geochemistry, 38, 91–180.

Guillemin, C. and Protas, J. (1959) Ianthinite et wyartite. Bulletin de Minéralogie, 82, 80–86.

Hawthorne, F.C., Finch, R.J., and Ewing, R.C. (2006) The crystal structure of dehydrated wyartite, $Ca(CO_3)[U^{5+}(U^{6+}O_2)_2O_4(OH)](H_2O)_3$. Canadian Mineralogist, 44, 1379–1385, https://doi.org/10.2113/gscanmin.44.6.1379.

Isbill, S.B., Shields, A.E., Niedziela, J.L., and Miskowiec, A.J. (2022) Density functional theory investigations into the magnetic ordering of U_3O_8. Physical Review Materials, 6, 104409, https://doi.org/10.1103/PhysRevMaterials.6.104409.

Kirkegaard, M.C., Niedziela, J.L., Miskowiec, A., Shields, A.E., and Anderson, B.B. (2019a) Elucidation of the Structure and Vibrational Spectroscopy of Synthetic Metaschoepite and Its Dehydration Product. Inorganic Chemistry, 58, 7310–7323, https://doi.org/10.1021/acs.inorgchem.9b00460.

Kirkegaard, M.C., Spano, T.L., Ambrogio, M.W., Niedziela, J.L., Miskowiec, A., Shields, A.E., and Anderson, B.B. (2019b) Formation of a uranyl hydroxide hydrate via hydration of $[(UO_2F_2)(H_2O)]_7{\cdot}4H_2O$. Dalton Transactions: An International Journal of Inorganic Chemistry, 48, 13685–13698, https://doi.org/10.1039/C9DT02835H.

Klingensmith, A.L., Deely, K.M., Kinman, W.S., Kelly, V., and Burns, P.C. (2007) Neptunium incorporation in sodium-substituted metaschoepite. American Mineralogist, 92, 662–669, https://doi.org/10.2138/am.2007.2350.

Lin, D.H.M., Manara, D., Varga, Z., Berlizov, A., Fanghänel, T., and Mayer, K. (2013) Applicability of Raman spectroscopy as a tool in nuclear forensics for analysis of uranium ore concentrates. Radiochimica Acta, 101, 779–784, https://doi.org/10.1524/ract.2013.2110.

Lin, D.H.M., Manara, D., Lindqvist-Reis, P., Fanghänel, T., and Mayer, K. (2014) The use of different dispersive Raman spectrometers for the analysis of uranium compounds. Vibrational Spectroscopy, 73, 102–110, https://doi.org/10.1016/j.vibspec.2014.05.002.

Lu, G., Haes, A.J., and Forbes, T.Z. (2018) Detection and identification of solids, surfaces, and solutions of uranium using vibrational spectroscopy. Coordination Chemistry Reviews, 374, 314–344, https://doi.org/10.1016/j.ccr.2018.07.010.

Lussier, A.J., Lopez, R.A., and Burns, P.C. (2016) A revised and expanded structure hierarchy of natural and synthetic hexavalent uranium compounds. Canadian Mineralogist, 54, 177–283, https://doi.org/10.3749/canmin.1500078.

Miller, M., Burns, P., Ewing, R., and Finch, R. (1997) Transuranium element incorporation into the β-U_3O_8 uranyl sheet. MRS Proceedings, 465, 581.

Miskowiec, A., Niedziela, J.L., Spano, T.L., Ambrogio, M.W., Finkeldei, S., Hunt, R., and Shields, A.E. (2019) Additional complexity in the Raman spectra of U_3O_8. Journal of Nuclear Materials, 527, 151790, https://doi.org/10.1016/j.jnucmat.2019.151790.

Miskowiec, A., Spano, T., Hunt, R., Shields, A.E., Niedziela, J., and Finkeldei, S. (2020) Structural features of solid-solid phase transitions and lattice dynamics in U_3O_8. Physical Review Materials, 4, 093610, https://doi.org/10.1103/PhysRevMaterials.4.093610.

Miskowiec, A., Spano, T., Brubaker, Z.E., Niedziela, J., Abernathy, D., Hunt, R.D., and Finkeldei, S. (2021) Antiferromagnetic ordering and possible lattice response to dynamic uranium valence in U_3O_8. Physical Review B, 103, 205101, https://doi.org/10.1103/PhysRevB.103.205101.

Miskowiec, A., Spano, T., Hunt, R., and Kurley, J. (2022) Optical vibrational spectra of β-U_3O_8. Journal of Nuclear Materials, 568, 153894, https://doi.org/10.1016/j.jnucmat.2022.153894.

Olds, T.A., Lussier, A.J., Petříček, V., Plášil, J., Kampf, A.R., Oliver, A.G., Burns, P.C., Dembowski, M., and Steele, I.M. (2023) Shinkolobweite, from the Shinkolobwe Mine, Democratic Republic of Congo: A New Mineral Containing Uranium in the Rare Pentavalent Oxidation State. The Canadian Journal of Mineralogy and Petrology, 61, 999–1020, https://doi.org/10.3749/2300003.

Plášil, J. (2017) Crystal structure of richetite revisited: Crystallographic evidence for the presence of pentavalent uranium. American Mineralogist, 102, 1771–1775.

Plášil, J., Kampf, A.R., Škoda, R., and Čejka, J. (2018) Nollmotzite, $Mg[U^{V}(U^{VI}O_2)_2O_4F_3]{\cdot}4H_2O$, the first natural uranium oxide containing fluorine. Acta Crystallographica Section B, 74, 362–369, https://doi.org/10.1107/S2052520618007321.

Ranasinghe, J.I., Malakkal, L., Jossou, E., Szpunar, B., and Szpunar, J.A. (2020) Comprehensive study on the electronic and optical properties of α-U_3O_8. Computational Materials Science, 171, 109264, https://doi.org/10.1016/j.commatsci.2019.109264.

Said, M., Perry, S.N., Benjamin, S.E., and Hixon, A.E. (2021) Formation of ammonium uranate on uranium dioxide during aging under controlled storage conditions. Journal of Nuclear Materials, 555, 153078, https://doi.org/10.1016/j.jnucmat.2021.153078.

Schwantes, J.M., Corbey, J.F., and Marsden, O. (2022a) Exercise Celestial Skónis: Part 1–History, purpose, design and results of traditional forensic examinations of the 6th Collaborative materials exercise of the nuclear forensics International Technical Working Group. Forensic Chemistry, 29, 100424, https://doi.org/10.1016/j.forc.2022.100424.

——— (2022b) Exercise Celestial Skónis: Part 2–Emerging technologies and state of practice of nuclear forensic analyses demonstrated during the 6th Collaborative Materials Exercise of the Nuclear Forensics International Technical Working Group. Forensic Chemistry, 29, 100423.

Singh, Y., Viswanathan, R., Parashar, K., Srivastava, S., Ramesh Babu, P., and Parihar, P. (2014) Ianthinite: A rare hydrous uranium oxide mineral from Akkavaram, Andhra Pradesh, India. Journal of Earth System Science, 123, 15–19, https://doi.org/10.1007/s12040-013-0371-2.

Spano, T.L., Olds, T.A., McDonnell, M., Smith, R., Niedziela, J.L., Miskowiec, A., Kapsimalis, R., and Shields, A.E. (2023) CURIES: Compendium of uranium Raman and infrared experimental spectra. American Mineralogist, 108, 2219–2233, https://doi.org/10.2138/am-2022-8738.

Taylor, P., Wood, D.D., Owen, D.G., and Park, G.-I. (1991) Crystallization of U_3O_8 and hydrated UO_3 on UO_2 fuel in aerated water near 200 C. Journal of Nuclear Materials, 183, 105–114, https://doi.org/10.1016/0022-3115(91)90477-O.

Wen, X.-D., Martin, R.L., Scuseria, G.E., Rudin, S.P., Batista, E.R., and Burrell, A.K. (2013) Screened hybrid and DFT + U studies of the structural, electronic, and optical properties of U_3O_8. Journal of Physics. Condensed Matter: An Institute of Physics Journal, 25, 025501, https://doi.org/10.1088/0953-8984/25/2/025501.

Wojdyr, M. (2010) Fityk: A general purpose peak fitting program. Journal of Applied Crystallography, 43(5 1), 1126–1128.

Yun, Y., Rusz, J., Suzuki, M.-T., and Oppeneer, P. (2011) First-principles investigation of higher oxides of uranium and neptunium: U_3O_8 and Np_2O_5. Physical Review B: Condensed Matter and Materials Physics, 83, 075109, https://doi.org/10.1103/PhysRevB.83.075109.

Manuscript received January 17, 2025
Manuscript accepted July 15, 2025
Accepted manuscript online July 25, 2025
Manuscript Handled by Jennifer Kung

Endnotes:

[1]Deposit item AM-26-39759. Online Materials are free to all readers. Go online, via the table of contents or article view, and find the tab or link for supplemental materials.